

The decay curves of luminescence from Eu^{2+} in $\beta\text{-SiAlON}$ are effectively analyzed using the general-order kinetics formula

Yoriko Suda^{1,2}, Tsuyoshi Okuno², Takashi Takeda³, Kohsei Takahashi³ and Naoto Hirosaki³

¹ School of Engineering, Tokyo University of Technology, Hachioji, Tokyo 192-0982, Japan

² Department of Engineering Science, The University of Electro-Communications, Chofu, Tokyo 182-8585, Japan

³ Sialon Group, National Institute for Materials Science, Tsukuba, Ibaraki 305-0044, Japan

Email:

H57924d8@edu.teu.ac.jp and sudayoriko@uec.ac.jp

Received xxxxxx

Accepted for publication xxxxxx

Published xxxxxx

Abstract

Defects in phosphors affect not only luminescence intensity but also emission peak width, decay time, and afterglow. The green phosphor $\beta\text{-SiAlON}:\text{Eu}^{2+}$ exhibits the green emission of Eu^{2+} at 520 nm and the blue emission of nitrogen vacancies at 460 nm in time-resolved fluorescence measurements. The decay time of the intrinsic Eu^{2+} transition is 0.7 μs , but afterglow is detected from 50 μs to 0.01 s. This afterglow decay curve is the same for the green emission of Eu^{2+} and the blue emission of nitrogen vacancies, suggesting that the defect levels of the nitrogen vacancies affect the Eu^{2+} transition. The afterglow decay curves were analyzed using the formula of the general-order kinetics, $(1 + t/\tau_B)^{-n}$, where n is the decay power and τ_B is the decay time. This equation is generally used when analyzing afterglow on the order of seconds to hours but has not been examined systematically applied in samples with different concentrations of Eu^{2+} and concentrations on the order of nanoseconds to milliseconds. The decay power n is approximately 1 for all Eu^{2+} concentrations ($x = 0.001$ to 0.3) and undoped $\beta\text{-SiAlON}$. The decay time τ_B is correlated with the density of the nitrogen vacancies determined by electron spin resonance. Furthermore, the value of n is approximately 1 for 50 μs to 0.01 s and 0.3 for 1–1000 s. Thus, the luminescence mechanism of Eu^{2+} can be discussed by comparing n and τ_B obtained from the decay curves. In addition, several different Eu^{2+} -doped phosphors, namely $\text{SrAl}_2\text{O}_4:\text{Eu}^{2+}$, Dy^{3+} , $\text{CaAlSiN}_3:\text{Eu}^{2+}$, and $\text{CaS}:\text{Eu}^{2+}$, Tm^{3+} , are studied.

Keywords: luminescence, decay curve, afterglow, phosphor, SiAlON, europium

1. Introduction

White light-emitting diodes (LEDs) are widely used in our daily lives. Usually, white LEDs are packaged with green, yellow, orange, and red phosphors and combined with blue LEDs. These phosphors must be excited by blue or UV light

and have high efficiency. Therefore, various wide-gap phosphors have been developed. Nitrides and nitrogen oxides are suitable phosphors because they have high chemical and thermal stability [1]. However, various types of defects, such as nitrogen vacancies (V_N) and interstitial atoms, are inevitably included in wide-gap phosphors and affect their optical properties. Thus, it is necessary to identify the defect

types and concentrations for device development and improvement.

The green phosphor $\text{SrAl}_2\text{O}_4:\text{Eu}^{2+}$ emits a long afterglow due to oxygen vacancies. Green emission has an intrinsic decay time for Eu^{2+} , with a value of $\sim 1 \mu\text{s}$ [2,3]. In 2009, the intrinsic decay times of Eu^{2+} were measured in over 30 typical Eu^{2+} -doped phosphors, as shown in Figure 1 [4]. The relationship between emission wavelength and decay time is plotted. The intrinsic decay time increases as the emission wavelength increases [2-4]. The luminescence of long afterglow phosphors initially decreases with the intrinsic decay time of Eu^{2+} for $\sim 1 \mu\text{s}$, and then they show an afterglow on the order of seconds, minutes, or hours. This afterglow is caused by the sequential release of electrons temporarily trapped in defect levels [2,5,6]. Therefore, the density of the defect levels affects afterglow intensity.

The decay curve is often analyzed using the general-order kinetics equation for afterglow in the seconds to hours range. The afterglow intensity at time t is proportional to $(1 + t/\tau_B)^{-n}$ [2,5,6], where τ_B is the decay time and n is the decay power. In the case where n is ~ 1 , the decay formula is called the Becquerel decay formula [7,8]. $\text{SrAl}_2\text{O}_4:\text{Eu}^{2+}$ and various phosphors have a decay power n of ~ 1 [2,5,6,9-12]. However, this formula has not been used for analyzing decay curves in a time range shorter than 1 s. Herein, decay curves in the nanoseconds to milliseconds range are analyzed at different concentrations of Eu^{2+} and measurement temperatures, and compared in the seconds to minutes range.

$\text{Si}_{6-z}\text{Al}_z\text{O}_z\text{N}_{8-z}:\text{Eu}^{2+}$ (β -SiAlON: Eu^{2+}) is a phosphor that emits in the green region from 510 to 540 nm [1,13-21]. It has a broad excitation spectrum of Eu^{2+} and a narrow emission peak width. The absorption efficiency of 68% and external quantum efficiency of 50% were achieved in 2016 [1]. Only a limited number of Eu^{2+} ions in β -SiAlON is considered to contribute to green luminescence, and some improvement is possible. The phosphor has been developed not only for LEDs [13-15] but also for liquid crystal display backlights with narrower peak widths [16,17]. β -SiAlON:Eu phosphor-containing glass as a wavelength converter in solid-state lighting has also been studied [18,19]. Several methods have been reported to improve the phosphor properties, such as the combustion synthesis [20] and annealing of the surface amorphous layer [21].

It was reported that Eu^{2+} -doped phosphors have luminescence in the UV or blue region, which exhibited an afterglow of a few milliseconds in time-resolved fluorescence (TR-F) measurements using a nanosecond pulse laser [22-25]. The blue luminescence originates from defects, and its intensity is correlated with the defect density. The density of V_N in β -SiAlON: Eu^{2+} was obtained from electron spin resonance (ESR) measurements. The depths of the defect levels, as electron traps, were estimated based on thermoluminescence (TL) [23,24]. These values were close to

the depths of the Si_3N_4 defect level [26-34] and Al-doped Si_3N_4 or SiAlON defect level [35-38]. These reports showed that decay curves of the emission due to defects and those of the emission due to Eu^{2+} were similar, but they could not be quantified or compared [23,24].

In this paper, decay curves of luminescence in β -SiAlON: Eu^{2+} are studied using TR-F measurements. The decay curve of the luminescence intensity at its peak wavelength reflects the process of luminescence. TR-F reveals the intrinsic Eu^{2+} decay in the nanosecond to microsecond range, as shown in Figure 1. We focus on the microsecond to millisecond range to investigate the slow luminescence phenomena of both the blue emission from defect levels and the green emission of Eu^{2+} . In addition to the decay curve of Eu^{2+} , afterglow in the ranges of 0.05 μs to 0.01 s and 1–1000 s is analyzed using the general-order kinetics decay formula, for the first time. Only the two parameters τ_B and n are used to discuss electron kinetics for the luminescence and afterglow. The intrinsic decay time of Eu^{2+} is $\sim 1 \mu\text{s}$, so the emission longer than 5 μs is also denoted as afterglow in this paper. The intrinsic decay of Eu^{2+} is finished before this time.

2. Experimental

Samples were prepared using a previously described method (low oxygen firing conditions) [1,16,23,24]. Si_3N_4 , AlN, and Eu_2O_3 were mixed with a stoichiometric ratio of $\text{Si}_{6-z}\text{Al}_z\text{O}_z\text{N}_{8-z}:\text{Eu}^{2+}$ ($z = 0.03$). The Eu concentrations ($x = 0, 0.001\text{--}0.3$) correspond to the number of atomic ratios per unit cell for the host material crystal of β -SiAlON. Mixtures were fired at 2300 K for 2 h in a nitrogen atmosphere of 0.9 MPa. X-ray diffraction revealed that the low Eu-concentration samples ($x = 0, 0.001\text{--}0.01$) have a single phase [23,24]. In the high Eu-concentration samples ($x = 0.03\text{--}0.3$), 1%–14% $\text{Eu}_2\text{Si}_5\text{N}_8$ was detected [24]. $\text{Eu}_2\text{Si}_5\text{N}_8$ is a black crystal [39,40], which affected the overall color of our samples, appearing yellow to brown. No effect of $\text{Eu}_2\text{Si}_5\text{N}_8$ on the luminescence properties of high Eu-concentration samples is considered because the green phosphor β -SiAlON: Eu^{2+} and the black $\text{Eu}_2\text{Si}_5\text{N}_8$, which does not exhibit luminescence, form different particles.

The internal quantum efficiency (IQE) was measured at 300 K using an absolute photoluminescence quantum yield measurement system (C11347, Hamamatsu Photonics, Japan). For the TR-F measurements, a 266 nm Nd:YAG laser (Ultra CFR, Big Sky Laser Technologies Inc., MT, USA) was used as the excitation light source. The pulse width was 10 ns, and the repetition was 10 Hz. Spectra were measured using a monochromator (Spectra Pro 2300i, Princeton Instruments, NJ, USA) and a CCD detector (PI-Max, Princeton Instruments, NJ, USA) synchronized to the laser. A UV-cut filter (UV-31) was used to reduce the excitation light. Samples were set in a cryostat and measured at 15–300 K.

The afterglow measurement in the range of seconds to minutes was conducted using a different system from that of TR-F. The excitation light source was a high-pressure mercury lamp (254 nm), and the detector was a photomultiplier tube (R374, Hamamatsu Photonics, Japan). Afterglow was measured at 60 and 300 K using a cryostat.

The analysis of the emission decay curves was conducted using the following two equations. When the luminescence intensity during excitation is I_0 , the intensity at time t after stopping the excitation light is expressed as [1-3]:

$$I(t) = I_0 \exp\left(-\frac{t}{\tau}\right). \quad (1)$$

Equation (1) is known as the first-order kinetics formula. The value of τ is the decay time of emission ions (Eu^{2+}) in the phosphor.

After the excitation light is stopped and time increases, the decay curve can be expressed as:

$$I(t) = I_0 \exp\left(1 + \frac{t}{\tau_B}\right)^{-n}, \quad (2)$$

where the decay power is n and the decay time is τ_B [2,5,6,8]. Equation (2) represents the general-order kinetics, providing the second-order kinetics formula for $n = 2$. This equation is derived by integrating the elementary bimolecular reaction (electrons and holes) rate equation [8]. It is also known as the Becquerel decay formula for $n = 1$ [7,8]. The value of n represents the magnitude of the slope of a straight line when the decay curve is plotted on the log-log graph.

In the decay curve of phosphor luminescence, the decay power n in Equation (2) takes values between 0.5 and 2, which is considered ~ 1 [2,5,6,9-12]. Only the two parameters n and τ_B are needed to approximate the decay curve of the afterglow due to defect levels that trap carriers. Equation (2) is used as an empirical formula in this study to compare results and discuss defect levels for various samples.

3. Results and discussion

3.1 Samples and TR-F spectra

β -SiAlON: Eu^{2+} is a phosphor that emits green at 520 nm owing to the $4f^65d-4f^7$ transition of Eu^{2+} . The IQE of the sample with the Eu^{2+} concentration $x = 0.01$ was 53% under the excitation at 300 nm. This value is thought to be similar to the value of $\sim 70\%$ obtained for the commercial product, considering potential variations in the Eu^{2+} concentrations or firing conditions.

Figure 2 shows the TR-F spectra of β -SiAlON: Eu^{2+} at 15 K. The sample without Eu^{2+} ($x = 0$) has broad emission peaks at

320, 460, and 600 nm. The 460 nm blue emission peak is also detected in Eu-doped samples, but its emission intensity decreases with increasing Eu concentration. The emission from Eu^{2+} is detected as a broad 520 nm spectrum, overlapped by a group of line spectra. Line spectra at 590 and 615 nm represent emission from the intra $4f^6$ transition of Eu^{3+} [21,24]. Samples with a small ratio of Al and O ($z = 0.03$) have the zero-phonon line detected at 510 nm, and its phonon shifts at low temperatures [16,17,24].

Figure 3 shows the decay curves at 520 nm (indicated by the arrow in Figure 2) for the duration of $\sim 1 \mu\text{s}$ after stopping the excitation light. The sampling time is 5 ns and the temperature is 15 K. The decay time was the same $\tau = 0.7 \mu\text{s}$ in Equation (1), for various Eu concentrations. This value is the intrinsic decay time for the $4f^65d-4f^7$ transition of Eu^{2+} .

For the sample with the lowest Eu^{2+} concentration ($x = 0.001$), decay curves were measured over a wider time range. Figure 4 shows decay curves plotted in (a) semi-log and (b) log-log graphs, and the sampling time is displayed. In Figure 4(a), the decay curve becomes a straight line between $t = 0$ and $5 \mu\text{s}$. The slope corresponds to $\tau = 0.7 \mu\text{s}$ in Equation (1). In Figure 4(b), the decay curve of Equation (1) is shown as a thin black dotted curve, and the decay curve of Equation (2) is shown as a black dashed line. The magnitude of the slope corresponds to the decay power n [6], which is ~ 1 . The yellow symbols (500 ns) deviate from the dotted curve and decay with the dashed line after $t = 5 \mu\text{s}$. For the sampling time of $50 \mu\text{s}$, the value of the red symbols appears to be amplified at $t = 10^{-4}$ s. This is due to the normalization of the vertical axis in Figure 4. The pulse width of the excitation is 10 ns, so the initial normalized intensity has already decreased by decay for measurements longer than 50 ns. Between $t = 10^{-4}$ and 10^{-2} s in Figure 4(b), the red symbols follow a straight line. The straight line in the log-log graph is reproduced using Equation (2), and the magnitude of the slope corresponds to the decay power n [6], which is ~ 1 between $t = 10^{-4}$ and 10^{-2} s. The yellow symbols from $t = 10^{-5}$ to 10^{-4} s also follow a straight line with a slope of ~ 1 .

In Figure 4(b), the decay of the afterglow between $t = 1$ and 100 s is included. The measurement temperature for the afterglow was 60 K, which differs from the temperature of 15 K for TR-F. Both of the temperatures are far below 300 K, and no effect of different temperatures between 60 and 15 K is expected. Between $t = 1$ and 10 s, the data again follow a straight line with a slope of ~ 1 . The decay curve is reproduced by Equation (2) in the time ranges from $5 \mu\text{s}$ to 10 s. After 10 s, the decay line remains straight but the slope changes to ~ 0.3 .

The decay curve can be explained by different decay equations, and the luminescence mechanism is different depending on the time ranges. The initial decay before $t = 5 \mu\text{s}$ is caused by the intrinsic transition of Eu^{2+} according to Equation (1), and the afterglow is not intrinsic to Eu^{2+} .

3.2 Decay curves of β -SiAlON

The decay curves of blue and green emission in the millisecond range were investigated for β -SiAlON:Eu²⁺. The sample with the lowest Eu²⁺ concentration ($x = 0.001$) was measured. It had a green emission peak at 520 nm from Eu²⁺, as well as a broad blue emission at 460 nm, as shown in Figure 2. Figure 5 shows the decay curves for 0.01 s. The sampling time is 50 μ s, and the temperature is 15 K. The decay curve for the 460 nm emission of the sample without Eu²⁺ ($x = 0$) is also shown. Values in the vertical axis are normalized by the intensity at $t = 0$, where the intrinsic decay of Eu²⁺ ($\tau = 0.7 \mu$ s) is dominant for each decay curve. Thus, the intensity for 520 nm in Figure 5, at $t = 0.005$ s for example, corresponds to the emission intensity ratio of the afterglow to the intrinsic transition of Eu²⁺. In the decay curves of the semi-log graph in Figure 5(a), the intensity between $t = 0$ to 0.001 s is different, but the curves after $t = 0.001$ s for 460 and 520 nm are almost the same. Their decay curves are the same as the curve for 460 nm in the sample without Eu²⁺ ($x = 0$). Furthermore, the decay curves in the log-log graph in Figure 5(b) are all straight lines. The intensity decreases similarly, and the slope values are -0.7 to -1.1 . The decay power n in Equation (2) is determined from the slope. Then, the decay time τ_B in Equation (2) is chosen to match the respective decay curve. The results are shown in Figure 5(c). The coefficients of determination R^2 were 0.99 to 1, and thus the two parameters n and τ_B explain the decay curves well.

The blue luminescence of the sample without Eu²⁺ ($x = 0$) was due to transitions between defect levels ($\sigma_{\text{Si-Si}}^* \rightarrow V_N^{3+}$ or K^0 center) created by V_N [23,24]. In Figure 5(b), the intensity at 520 nm ($x = 0.001$) and 460 nm ($x = 0$) decreases with approximately the same slope (-1.0 and -1.1). This means that the Eu²⁺ emission at 520 nm decreases with the luminescence mechanism of the transitions at 460 nm between defect levels in the time range from 50 μ s to 0.01 s. This is not the intrinsic transition of Eu²⁺, but is caused by the transfer of electrons trapped in defect levels to the excited state of Eu²⁺. The electrons trapped in defect levels are the origin of the afterglow.

3.3 Eu concentration dependence of decay curves

As the Eu²⁺ concentration increased, the emission intensity of β -SiAlON:Eu²⁺ became stronger while the afterglow decreased [24]. In Figure 2, the width of the broad emission at 520 nm became wider and several sharp phonon lines, such as those at 510 and 530 nm, decreased as the Eu²⁺ concentration increased. The broad blue emission at 460 nm decreased with increasing Eu²⁺ concentration and disappeared above $x = 0.003$.

Figure 6 shows the Eu²⁺ concentration dependence of the decay curves for the 520 nm emission from Eu²⁺ at 15 K, plotted on the log-log graph. The dashed line represents the

decay curve calculated using Equation (2). The two parameters n and τ_B are shown in Table 1.

In Figure 6, the intensity at $t = 50 \mu$ s for the low Eu²⁺-concentration samples ($x = 0.001$ and 0.003) is larger than that for the other samples. After $t = 50 \mu$ s, the decay curves are almost the same for all Eu²⁺ concentrations. Decay curves are plotted as straight lines, and their slope values are close to $n = 1$.

In Figures 3 and 4, the emission decreased according to the first-order kinetics in Equation (1) between $t = 0$ and 5 μ s, and thereafter it decreased following Equation (2). The decay curves for various Eu²⁺ concentrations all have the same slope of ~ 1 , and thus they are compared by the value of τ_B . When n is the same, the value at $t = 50 \mu$ s increases as τ_B increases, as shown in Figure 6. The intensity in Figure 6 is normalized by the value at $t = 0$ s (the intrinsic Eu²⁺ transition), and thus the value at $t = 50 \mu$ s is regarded as the ratio of the afterglow component to the intrinsic transition of Eu²⁺.

Figure 7(a) shows the Eu²⁺ concentration dependence of the decay time τ_B in Equation (2). τ_B is 2 μ s for the lowest Eu²⁺ concentration ($x = 0.001$), but decreases by approximately one order of magnitude at higher Eu²⁺ concentrations. Figure 7(b) shows the Eu²⁺ concentration dependence of the emission intensity (afterglow intensity) at $t = 50 \mu$ s, in addition to the density of V_N . The V_N density was evaluated from the ESR signal intensity of the Si-dangling bonds [23]. The intrinsic decay of Eu²⁺ disappears at $t = 5 \mu$ s, as shown in Figure 4(a), so the intensity at $t = 50 \mu$ s in Figure 7(b) shows the intensity of the afterglow. The millisecond afterglow in Figure 6 involves the transfer of electrons trapped in defects to Eu²⁺, and its intensity is correlated with the density of V_N measured by ESR [22-24]. Figure 7(b) shows that the afterglow intensity at 50 μ s, and the density of V_N decreases at higher Eu²⁺ concentrations. The τ_B value relates to the afterglow intensity when the decay power n is nearly the same. The defect density is revealed based on the value of τ_B .

3.4 Temperature dependence of decay curves

The temperature dependence was investigated for the emission of β -SiAlON:Eu²⁺ ($x = 0.001$). Figure 8(a) shows variations of the emission spectra at 15–300 K. The broad blue emission at 460 nm is strong at 15 K but decreases with increasing temperature. The emission at 520 nm from Eu²⁺ is composed of sharp phonon lines at 510, 515, 520, and 535 nm and a broad peak at 520 nm at low temperatures. With increasing temperature, the line spectrum emission decreases.

Figure 8(b) compares decay curves of the blue emission, which is related to defects. The decay curves calculated using Equation (2) are represented by dashed lines. Decay parameters n and τ_B are shown in Table 2. The log-log graph in Figure 8(b) shows straight lines with slope values of $n = 0.7$ – 0.8 at 15 and 100 K. At temperatures higher than 200 K,

the decay slopes were $n = 1.4$ until it disappeared into the background after $t = 0.0005$ s.

Figure 8(c) shows the temperature dependence of the decay curves for the green emission at 520 nm of Eu^{2+} . All decay curves are plotted as straight lines on the log-log graph. The value of their slopes is ~ 1 , and the value of n increases with increasing temperature, while the decay becomes faster. The decay parameters n and τ_B fitted for Equation (2) are included in Table 2.

Figure 9 shows the afterglow measured between $t = 1$ and 1000 s using another method, and the 520 nm emission of Eu^{2+} is detected. Almost no afterglow is observed in the semi-log graph after $t = 500$ s in Figure 9(a), and the decay curves are plotted as straight lines in the log-log graph in Figure 9(b). Furthermore, the slope is $n = 1.1$ between 1 and 10 s at 60 K. This value is similar to that obtained in the time range of 50 μs to 0.01 s in Figures 6, 8(b), and 8(c). This decay with a slope of ~ 1 is related to V_N in Figure 7, and the decay between 1 and 10 s at 60 K is also considered to be related to V_N . The slope of $n = 0.3$ is obtained between 10 and 500 s at 60 K and 1 and 500 s at 300 K.

3.5 Decay curves and trap levels

Decay curves in the time range of 50 μs to 0.01 s measured by TR-F were analyzed using the general-order kinetics of Equation (2). Only two parameters n and τ_B are used in Equation (2) in Figures 4–6, 8, and 9, in addition to Tables 1 and 2. The value of ~ 1 for n is often reported for various host crystals and luminescent ions [5,6,9–12]. In $\text{SrAl}_2\text{O}_4:\text{Eu}^{2+}$, Dy^{3+} , the oxygen defects cause the long afterglow, and the decay curve in the time range of minutes to hours is reproduced using a slope of ~ 1 [9,10].

The value of $n = 2$ in Equation (2) is applied for the one-electron trap level and the one-center model [8], as shown in the energy diagram of Figure 10(a). The energy difference between the bottom of the conduction band and the trap level is denoted as $\Delta\epsilon$. The electrons detrapped from the trap level are transferred to the luminescent Eu^{2+} ions, and then the emission transitions occur from the excited level $4f^65d^1$ to the ground level $4f^7$. When the trapping and detrapping take place between the electron trap and Eu^{2+} , a decay curve of $n = 2$ appears [5,6,8]. It has been empirically shown that the decay curve is proportional to $1/t$, which is attributed to repeated detrapping and retrapping, or tunneling [41–43]. Because there is a distribution of trap levels, simulations for various distributions (i.e., uniform, exponential, Gaussian) have been reported [6,8,44,45]. When there are many electron trap levels with a distribution in the energy difference $\Delta\epsilon$, as shown in Figure 10(b), the decay power is considered to be ~ 1 [5,6,8,41–45].

Figure 10(c) shows the energy level schematic for the emission of $\beta\text{-SiAlON}:\text{Eu}^{2+}$. There are several trap levels for V_N at the energy depth of 0.2–0.8 eV, which was previously

determined using the TL method [23,24]. Before transferring from V_N to Eu^{2+} , electrons might repeat detrapping and retrapping between the levels of V_N . Tunneling between V_N and Eu^{2+} also occurs between Eu^{2+} and some V_N close to Eu^{2+} . These complicated phenomena may change the decay power from $n = 2$ to ~ 1 . Although it is not possible to determine the distribution of $\Delta\epsilon$ using Equation (2) in this paper, the decay power is used to compare the decay kinetics among similar material compositions. Further studies are required to clarify how the trapping, tunneling, and distribution of $\Delta\epsilon$ change the decay power. However, when comparing the same material compositions, as in this work, it is possible to compare the decay power.

In Figure 6, the decay power n did not change with the variation in Eu^{2+} concentration, suggesting that the luminescence mechanism does not change with Eu^{2+} concentration. The emission of Eu^{2+} in Figures 8(c) and 9(b) exhibits almost the same value of n as that for the blue emission in Figure 8(b). This suggests that the green emission of Eu^{2+} and the blue emission of V_N are affected by the same trapping and detrapping phenomena depicted in Figure 10(c). In Figures 8(c) and 9(b), n was ~ 1 and decreased to 0.3 after $t = 10$ s. The value was also 0.3 when the temperature was raised to 300 K. This suggests that the trapping level for the afterglow has changed, and thus the luminescence mechanism has changed with time or temperature. When the temperature increases, shallow V_N levels do not trap electrons because of the excess thermal energy. The decrease in n with time is caused by the absence of electrons in shallow trap levels. At high temperatures, electrons are located only in the relatively deep trap levels and are considered to be detrapped over a slow time scale.

The blue emission of defect levels was only observed at low Eu^{2+} concentrations and low temperatures. Analyzing the decay curve of the Eu^{2+} emission helps to identify the properties of the defect transition. Moreover, examining the two parameters n and τ_B in Equation (2) elucidates the luminescence mechanism and the defect density. This method is useful for developing new phosphors and improving their properties, especially for long afterglow phosphors where defect concentration is more important.

3.6 Decay curves of Eu^{2+} -doped phosphors

In the previous subsections, the decay curves for the emission of $\beta\text{-SiAlON}:\text{Eu}^{2+}$ in the time ranges of 50 μs to 0.01 s and 1–1000 s were obtained using the general-order kinetics of Equation (2). In this subsection, we show that Equation (2) can reproduce decay curves of different Eu^{2+} -doped phosphors. $\text{BaMgAl}_{10}\text{O}_{17}(\text{BAM}):\text{Eu}^{2+}$, $\text{SrAl}_2\text{O}_4:\text{Eu}^{2+}$, Dy^{3+} , $\alpha\text{-SiAlON}:\text{Eu}^{2+}$, $\text{Ca}_2\text{Si}_5\text{N}_8:\text{Eu}^{2+}$, $\text{CaAlSiN}_3:\text{Eu}^{2+}$, and $\text{CaS}:\text{Eu}^{2+}$, Tm^{3+} [4,22,25] were studied. Decay curves measured by TR-F with 266 nm laser excitation at 15 K are shown in Figure 11. All luminescence intensities were measured at the emission

wavelength of Eu^{2+} , and the decay parameters n and τ_B are shown in Table 3. Initially, until $t = 0.005$ s, CaS:Eu^{2+} , Tm^{3+} shows a slow decay and a slope of -0.8 , but the slope changes to -1.1 after $t = 0.005$ s. All other decay curves follow straight lines on the log-log graph and have a slope of -1.0 (decay power $n = 1.0$). The general-order kinetics is used not only for defects due to V_N (SiAlON and nitrides) but also for oxygen vacancies (BAM and $\text{SrAl}_2\text{O}_4\text{:Eu}^{2+}$, Dy^{3+}) and sulfur vacancies (CaS:Eu^{2+} , Tm^{3+}).

The decay curves of the afterglow excited using a 254 nm Hg lamp were measured, as shown in Figure 12. Emission intensity was detected using a photomultiplier tube at 300 K. The decay parameters n and τ_B are shown in Table 3. The decay power n is smaller (0.6–0.8) and decay is slower in the longer time region shown in Figure 12 than that shown in Figure 11. This suggests that the time scales of trapping used for afterglow change from microseconds to milliseconds and from seconds to minutes. $\alpha\text{-SiAlON:Eu}^{2+}$ exhibits an n of 0.4, which is approximately the same as $n = 0.3$ for $\beta\text{-SiAlON:Eu}^{2+}$. For CaS:Eu^{2+} , Tm^{3+} , the slope changes at $t = 0.003$ s in Figure 11 and $t = 100$ s in Figure 12. CaS:Eu^{2+} , Tm^{3+} is co-doped with Tm^{3+} , and electrons in the defect level are affected by Tm^{3+} before transferring to Eu^{2+} [25]. This co-doping is possibly the origin of the change of the decay power n in CaS:Eu^{2+} , Tm^{3+} . BAM has no afterglow in this time range.

The values of the decay power n that are slightly smaller than 1, as shown in Table 3 for 1–1000 s, are often reported for long afterglow phosphors. In the green phosphor $\text{Y}_3\text{Al}_2\text{Ga}_3\text{O}_{12}\text{:Ce}^{3+}$, Yb^{3+} , afterglow intensity plotted in a log-log graph exhibits a change in the value of n , from ~ 0.5 at 60 s to 0.8 at 300,000 s [46]. Similarly, the value for the red phosphor $(\text{Sr}, \text{Ca})\text{AlSiN}_3\text{:Eu}^{2+}$ changes from 0.7 at 10 s to 1 at 10,000 s [47]. In $\text{CaAl}_2\text{O}_4\text{:Eu}$, Nd, TL experiments with varying excitation duration and varying excitation temperatures helped to clarify the distribution of trap depths in a violet afterglow phosphor [6]. A Gaussian-shaped distribution from 0.7 to 1.2 eV was evaluated, and the decay power n of 0.7 at 100 s and 1.28 at 40,000 s was observed in the log-log graph of the afterglow intensity. Similar TL results are expected for the phosphors shown in Table 3.

In all of the phosphors in Table 3, the two parameters n and τ_B of the general-order kinetics can reproduce the decay curves of the afterglow, after the intrinsic decay of Eu^{2+} disappears (at ~ 5 μs in Figure 4). The values in the general-order kinetics among different materials may be used for discussing the luminescence mechanism and afterglow, considering results from different measurements, such as ESR (Figure 7) or TL.

4. Conclusions

For $\beta\text{-SiAlON:Eu}^{2+}$, the decay curves in the time range of 5 ns to 0.01 s were studied by TR-F. The broad blue emission at 460 nm was related to defect levels, and the decay curves

were reproduced using the general-order kinetics formula. The afterglow intensity at time t was proportional to $(1 + t/\tau_B)^{-n}$. The decay power n of the blue emission due to V_N changed from 0.7 at 15 K to 1.4 at 300 K. The green emission of Eu^{2+} at 520 nm showed an intrinsic decay time $\tau = 0.7$ μs in the time range of 0–5 μs . After $t = 5$ μs , the decay curve exhibited the same shape as that of the blue emission, and a millisecond-range afterglow was observed. The decay power for the afterglow of Eu^{2+} was also ~ 1 . The same mechanism is considered to govern both the blue emission and afterglow of Eu^{2+} .

Decay curves among the samples with different concentrations of Eu^{2+} ($x = 0, 0.001\text{--}0.3$) were normalized by the intensity at $t = 0$, where the intrinsic decay of Eu^{2+} was dominant. When the decay power n was almost the same, as in the present case of ~ 1 , τ_B corresponded to the ratio of the afterglow intensity to the intensity of the intrinsic transition of Eu^{2+} . The value of τ_B decreased from 2 μs for $x = 0.001$ to 0.3 μs for $x = 0.3$. This tendency was the same for the signal intensity of V_N in ESR or the density of V_N . The afterglow of Eu^{2+} is ascribed to defect levels of V_N .

The decay curves for the emission of Eu^{2+} in multiple host phosphor crystals were measured and analyzed using the formula $(1 + t/\tau_B)^{-n}$. In the time range between 50 μs and 0.01 s, the decay power was ~ 1 for all six Eu^{2+} -doped phosphors studied herein. In the time range between 1 s and 1000 s, a slightly smaller value of 0.4–0.8 was obtained for the decay power. The results suggest that the luminescence mechanism of Eu^{2+} changed with time, and the trapped levels for afterglow changed from microseconds to milliseconds and from seconds to minutes. Therefore, the general-order kinetics analysis of the decay curve is an effective method for investigating the defect density and luminescence mechanisms.

Acknowledgments

We thank Robert Ireland, PhD, from Edanz (<https://jp.edanz.com/ac>) for editing a draft of this manuscript.

References

- [1] Xie R J, Li Y Q, Hiroaki N and Yamamoto H 2016 Nitride phosphors and solid-state lighting *CRC Press*
- [2] Shionoya S, Yen W M, and Yamamoto H 2018 Phosphor handbook *CRC press*
- [3] Poort S H M, Meyerink A and Blasse G 1997 Lifetime measurements in Eu^{2+} -doped host lattices *Journal of Physics and Chemistry of Solids* **58.9** 1451-1456
- [4] Suda Y and Yamamoto H 2009 Effects of host crystals on transition probability of Eu^{2+} luminescence *The 54th spring meeting of the Japan Society of Applied Physics* 31p-P11-19 (in Japanese)
- [5] Van den Eeckhout K, Smet P F and Poelman D 2010 Persistent luminescence in Eu^{2+} -doped compounds: a review *Materials* **3.4** 2536-2566

- [6] Van den Eeckhout K, Bos A J, Poelman D and Smet P F 2013 Revealing trap depth distributions in persistent phosphors *Physical Review B* **87.4** 045126
- [7] E. Becquerel 1867 La lumière, ses causes et ses effets Vol. 1 *Firmin Didot frères, fils et cie*
- [8] Berberan-Santos M N, Bodunov E N and Valeur B 2005 Mathematical functions for the analysis of luminescence decays with underlying distributions: 2. Becquerel (compressed hyperbola) and related decay functions *Chemical Physics* **317.1** 57-62
- [9] Chernov V, Meléndrez R, Pedroza-Montero M, Yen W M and Barboza-Flores M 2008 The behavior of thermally and optically stimulated luminescence of $\text{SrAl}_2\text{O}_4:\text{Eu}^{2+}$, Dy^{3+} long persistent phosphor after blue light illumination *Radiation Measurements* **43.2-6** 241-244
- [10] Ji Z, Tian S, Chen W, Kong Z and Wu J 2013 Enhanced long lasting persistent luminescent $\text{SrAl}_2\text{O}_4:\text{Eu}$, Dy ceramics prepared by electron beam bombardment *Radiation Measurements* **59** 210-213
- [11] Kitauro M, Sato A, Kamada K, Ohnishi A and Sasaki M 2014 Phosphorescence of Ce-doped $\text{Gd}_3\text{Al}_2\text{Ga}_3\text{O}_{12}$ crystals studied using luminescence spectroscopy *Journal of Applied Physics* **115.8** 083517
- [12] Brito H F, Hölsä J, Jungner H, Laamanen T, Lastusaari M, Malkamäki M and Rodrigues L C 2012 Persistent luminescence fading in $\text{Sr}_2\text{MgSi}_2\text{O}_7:\text{Eu}^{2+}, \text{R}^{3+}$ materials: a thermoluminescence study *Optical Materials Express* **2.3** 11232-11240
- [13] Xie R J, Hirosaki N, Li H L, Li Y Q and Mitomo M 2007 Synthesis and Photoluminescence Properties of β -sialon: $\text{Eu}^{2+}(\text{Si}_{6-z}\text{Al}_z\text{O}_8\text{N}_{8-z}:\text{Eu}^{2+})$: A Promising Green Oxynitride Phosphor for White Light-Emitting Diodes *Journal of the Electrochemical Society* **154.10** J314
- [14] Xie R J, Hirosaki N, Sakuma K and Kimura N 2008 White light-emitting diodes (LEDs) using (oxy) nitride phosphors *Journal of Physics D: Applied Physics* **41.14** 144013
- [15] Kimoto K, Xie R J, Matsui Y, Ishizuka K and Hirosaki N 2009 Direct observation of single dopant atom in light-emitting phosphor of β -SiAlON: Eu^{2+} *Applied Physics Letters* **94.4** 041908
- [16] Takahashi K, Xie R J and Hirosaki N 2011 Toward higher color purity and narrower emission band β -sialon: Eu^{2+} by reducing the oxygen concentration *Electrochemical and Solid-State Letters* **14.11** E38-E40
- [17] Takahashi K, Yoshimura K, Harada M, Tomomura Y, Takeda T, Xie R J and Hirosaki N 2012 On the origin of fine structure in the photoluminescence spectra of the β -sialon: Eu^{2+} green phosphor *Science and Technology of Advanced Materials* **13** 015004
- [18] Zhu Q Q, Wang X J, Wang L, Hirosaki N, Nishimura T, Tian Z F, Li Q, Xu Y Z, Xu X and Xie R J 2015 β -Sialon: Eu phosphor-in-glass: a robust green color converter for high power blue laser lighting *Journal of Materials Chemistry C* **3.41** 10761-10766
- [19] Yoshimura K, Fukunaga H, Izumi M, Harada M, Takahashi K, Segawa H, Xie R J and Hirosaki N 2017 Optical properties of green-emitting β -sialon: Eu phosphor-containing silica glasses and their deterioration mechanism *Japanese Journal of Applied Physics* **56.6** 2017 060302
- [20] Ge Y, Chen Y, Sun S, Tian Z, Zhang J and Xie Z 2016 The Eu^{2+} -concentration dependence of photoluminescence behaviors in β -SiAlON: Eu^{2+} green phosphors prepared by combustion synthesis *Ceramics International* **42.15** 17901-17904
- [21] Li S, Wang L, Tang D, Cho Y, Liu X, Zhou X, Lu L, Zhang L, Takeda T, Hirosaki N and Xie R J 2018 Achieving high quantum efficiency narrow-band β -sialon: Eu^{2+} phosphors for high-brightness LCD backlights by reducing the Eu^{3+} luminescence killer *Chemistry of Materials* **30.2** 494-505
- [22] Suda Y, Kamigaki Y and Yamamoto H 2018 Blue emission in photoluminescence spectra of the red phosphor $\text{CaAlSiN}_3:\text{Eu}^{2+}$ at low Eu^{2+} concentration *Journal of Applied Physics* **123.16** 16154
- [23] Suda Y, Kamigaki Y, Miyagawa H, Takeda T, Takahashi K and Hirosaki N 2020 Luminescence and afterglow due to defects in β -SiAlON crystal powder *Journal of Physics D: Applied Physics* **53.16** 165108
- [24] Suda Y, Kamigaki Y, Miyagawa H, Takeda T, Takahashi K and Hirosaki N 2020 Effects of Eu^{2+} on the luminescence and afterglow that arise from defects in β -SiAlON: Eu^{2+} *Journal of Physics D: Applied Physics* **54.6** 065102
- [25] Suda Y, Tamura Y, Yamaguchi S, Nanai Y and Okuno T 2021 Red afterglow and luminescence arising from defects in $\text{CaS}:\text{Eu}^{2+}$, Tm^{3+} *Journal of Physics D: Applied Physics* **54.41** 415103
- [26] Robertson J 1991 Electronic structure of silicon nitride *Philosophical Magazine B* **63.1** 47-77
- [27] Grün R 1979 The crystal structure of β - Si_3N_4 : structural and stability considerations between α - and β - Si_3N_4 *Acta Crystallographica Section B: Structural Crystallography and Crystal Chemistry* **35.4** 800-804
- [28] Fujita S and Sasaki A 1985 Dangling bonds in memory-quality silicon nitride films *Journal of the Electrochemical Society* **132.2** 398
- [29] Munakata F, Matsuo K, Furuya K, Akimune Y, Ye J and Ishikawa I 1999 Optical properties of single crystals grown from a Si melt in N_2 *Applied Physics Letters* **74.23** 3498-3500
- [30] Aozasa H, Fujiwara I and Kamigaki Y 2007 Analysis of carrier traps in silicon nitride film with discharge current transient spectroscopy, photoluminescence, and electron spin resonance *Japanese Journal of Applied Physics* **46.9R** 5762
- [31] Grillo M E, Elliott S D and Freysoldt C 2011 Native defects in hexagonal β - Si_3N_4 studied using density functional theory calculations *Physical Review B* **83.8** 085208
- [32] Takeda T, Xie R J and Hirosaki N 2012 Local structure analysis in nitride and oxynitride phosphors *ECS Journal of Solid State Science and Technology* **2.2** R3132-R3137
- [33] Zhu W, McEntire B, Enomoto Y, Boffelli M and Pezzotti G 2015 Point-Defect Populations As Induced by Cation/Anion Substitution in β - Si_3N_4 Lattice: A Cathodoluminescence Study *The Journal of Physical Chemistry C* **119.6** 3279-3287
- [34] Zhang L, Jin H, Yang W, Xie Z, Miao H and An L 2005 Optical properties of single-crystalline α - Si_3N_4 nanobelts *Applied Physics Letters* **86.6** 061908
- [35] Gao F, Wang Y, Zhang L, Yang W and An L 2010 Optical Properties of Heavily Al-Doped Single-Crystal Si_3N_4 Nanobelts *Journal of the American Ceramic Society* **93.5** 1364-1367
- [36] Gan L, Mao Z Y, Zeng X H, Zhang Y Q, Zhao Y, Xu F F, Zhu Y C and Liu X J 2014 The origin of bimodal luminescence of β -SiAlON: Eu^{2+} phosphors as revealed by fluorescence microscopy and cathodoluminescence analysis *Materials Research Bulletin* **51** 205-209
- [37] Grillo M E, Elliott S D, Rodriguez J, Añez R, Coll R, Suhane D S, Breuil A L, Arreggini A, Degraeve R, Shariq A, Beyer V and Czernohorsky M 2014 First-principles study of oxygen and aluminum defects in β - Si_3N_4 : Compensation and charge trapping *Computational Materials Science* **81** 178-183
- [38] Wang S, Liu X, Qu B, Song Z, Wang Z, Zhang S, Wang F, Geng W T and Liu Q 2019 Green persistent luminescence and the electronic structure of β -Sialon: Eu^{2+} *Journal of Materials Chemistry C* **7.40** 12544-12551
- [39] Huppertz H and Schnick W 1997 $\text{Eu}_2\text{Si}_5\text{N}_8$ and $\text{EuYbSi}_4\text{N}_7$ The first nitridosilicates with a divalent rare earth metal *Acta Crystallographica Section C: Crystal Structure Communications* **53.12** 1751-1753

- [40] Höppe H A, Trill H, Mosel B D, Eckert H, Kotzyba G, Pöttgen R and Schnick W 2002 Hyperfine interactions in the 13 K ferromagnet $\text{Eu}_2\text{Si}_5\text{N}_8$ *Journal of Physics and Chemistry of Solids* **63.5** 853-859
- [41] Randall J T and Wilkins M H F 1945 Phosphorescence and electron traps II The interpretation of long-period phosphorescence *Proceedings of the Royal Society of London, Series A Mathematical and Physical Sciences* **184.999** 390-407
- [42] Medlin W L 1961 Decay of phosphorescence from a distribution of trapping levels *Physical Review* **123.2** 502
- [43] Avouris P and Morgan T N 1981 A tunneling model for the decay of luminescence in inorganic phosphors: The case of $\text{Zn}_2\text{SiO}_4\text{:Mn}$ *The Journal of Chemical Physics* **74. 8** 4347-4355
- [44] Hornyak W F and Franklin A D 1988 Single level isothermal TL-decay (with energy level distribution and retrapping) *International Journal of Radiation Applications and Instrumentation, Part D Nuclear Tracks and Radiation Measurements* **14. 1-2** 81-89
- [45] Hornyak W F and Chen R 1989 Thermoluminescence and phosphorescence with a continuous distribution of activation energies *Journal of Luminescence* **44. 1-2** 73-81
- [46] Ueda J, Miyano S and Tanabe S 2018 Formation of deep electron traps by Yb^{3+} codoping leads to super-long persistent luminescence in Ce^{3+} -doped yttrium aluminum gallium garnet phosphors *ACS Applied Material Interfaces* **10** 20652-20660
- [47] Liu X, Song Z, Wang S and Liu Q 2019 The red persistent luminescence of $(\text{Sr,Ca})\text{AlSiN}_3\text{:Eu}^{2+}$ and mechanism different to $\text{SrAl}_2\text{O}_4\text{:Eu}^{2+},\text{Dy}^{3+}$ *Journal of Luminescence* **208** 313-321

Figure captions

Figure 1. Relation between luminescence energy E and intrinsic decay time τ in typical Eu^{2+} -doped phosphors [4]. All samples are measured at 10–15 K using an excitation laser wavelength of 266 nm.

Figure 2. TR-F spectra of $\beta\text{-SiAlON:Eu}^{2+}$ at 15 K. The luminescence during 50 μs from the excitation is integrated. The intensities for the samples including Eu^{2+} (without Eu^{2+}) are normalized using the value at 520 nm (460 nm).

Figure 3. Decay curves of the luminescence at 520 nm for $\beta\text{-SiAlON:Eu}^{2+}$. The sampling time is 5 ns, and the temperature is 15 K. The Eu concentration is $x = 0.001$ to 0.3. The decay curves are normalized using the luminescence intensity at $t = 0$. The decay time $\tau = 0.7 \mu\text{s}$ in Equation (1) is shown by the dashed line.

Figure 4. Decay curves of the luminescence at 520 nm for $\beta\text{-SiAlON:Eu}^{2+}$. The temperature is 15 K. Eu concentration is $x = 0.001$. (a) Semi-log plots and (b) log-log plots are shown. The sampling times are 5 ns (green), 50 ns (blue), 500 ns (yellow), 50 μs (orange) and 1 s (gray). Data with a sampling time of 1 s is measured with a 254 nm Hg lamp for excitation, a photomultiplier tube as a detector, and a temperature of 60 K. The thin dotted line is drawn by using Equation (1) with the intrinsic decay time of $\tau = 0.7 \mu\text{s}$. The dashed lines represent the calculation using Equation (2) with the decay power $n = 1$.

Figure 5. Decay curves of luminescence at 460 nm (blue triangles) and 520 nm (green squares) of $\beta\text{-SiAlON:Eu}^{2+}$ ($x = 0.001$). The decay curve for the sample without Eu ($x = 0$) is shown by the purple circles. Measurements are conducted at 15 K. The sampling time is 50 μs . (a) Semi-log plots and (b) log-log plots are shown. In (c), curves using Equation (2) to fit the data in (a) and (b) are drawn. The two parameters n and τ_B in Equation (2) are shown in the figures.

Figure 6. Decay curves for luminescence of $\beta\text{-SiAlON:Eu}^{2+}$ for different Eu concentrations at 15 K. Decay curves obtained at 520 nm are plotted on the log-log graph. The Eu concentrations ($x = 0.001$ to 0.3) are indicated. The numbers in the parentheses indicate the slopes of the log-log plots. The dashed lines represent the calculation using Equation (2). The decay parameters are shown in Table 1.

Figure 7. (a) Eu concentration (x) dependence of $\beta\text{-SiAlON:Eu}^{2+}$ of the decay time τ_B in Equation (2). (b) The luminescence intensity at $t = 50 \mu\text{s}$ in Figure 6 is shown on the left y-axis as afterglow intensity (green triangles). The defect density of nitrogen vacancies (V_N) determined from the ESR

signal intensity of the Si-dangling bond (pink squares) is shown on the right y-axis [24].

Figure 8. (a) TR-F spectra of $\beta\text{-SiAlON:Eu}^{2+}$ ($x = 0.001$). The measurement temperature is 15–300 K, and the sampling time is 50 μs . Decay curves obtained at (b) 460 and (c) 520 nm are plotted on the log-log graph. The slope value for the line is shown in parentheses. The dashed lines represent the calculations using Equation (2). The decay parameters are shown in Table 2.

Figure 9. Decay curves of afterglow intensity of $\beta\text{-SiAlON:Eu}^{2+}$ at 60 and 300 K. The excitation wavelength is 254 nm. (a) Semi-log plots and (b) log-log plots are shown. The black dashed line indicates the background level. The blue (60 K) and orange (300 K) dashed lines represent the calculations using Equation (2), and the slope value for the line is shown in (b).

Figure 10. Schematic of energy levels for luminescence caused by electron trapping. These figures show the structure near the conduction band (CB). Emission proceeds by the transfer of electrons to the luminescent ions Eu^{2+} . (a) There is one trap level at depth $\Delta\epsilon$. (b) There are many trap levels, and the depths have various distributions. (c) Defect level (V_N) transitions in $\beta\text{-SiAlON:Eu}^{2+}$ and emission of Eu^{2+} . Trapping and detrapping occur at multiple trap levels, which have some distance from Eu^{2+} . For a trap level adjacent to Eu^{2+} , detrapping and transfer to Eu^{2+} , as well as tunneling between the trap and Eu^{2+} , may occur.

Figure 11. Decay curves of Eu^{2+} -doped phosphors at 15 K. Luminescence intensity is detected at the wavelength of the transition of Eu^{2+} in the corresponding phosphors. The excitation laser wavelength is 266 nm. The decay parameters are shown in Table 3. $\text{BaMgAl}_{10}\text{O}_{17}$ has no afterglow in this time range, and its results correspond to the background level, which differs slightly in this figure. The intensity is normalized by the emission value at $t = 0$ s under the excitation for each phosphor.

Figure 12. Decay curves for the afterglow of Eu^{2+} -doped phosphors. The measurement temperature is 300 K, and the excitation wavelength is 254 nm, using a Hg lamp. The decay parameters are shown in Table 3.

Figures

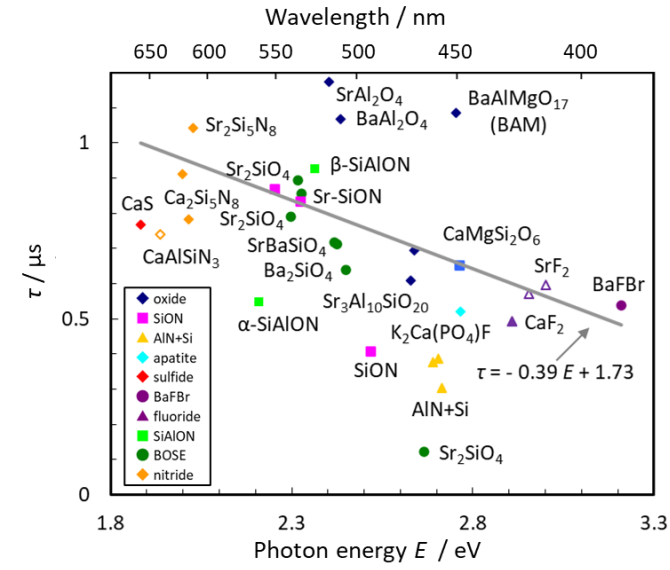


Figure 1.

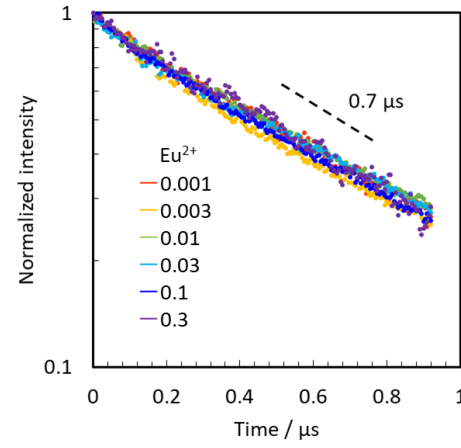


Figure 3.

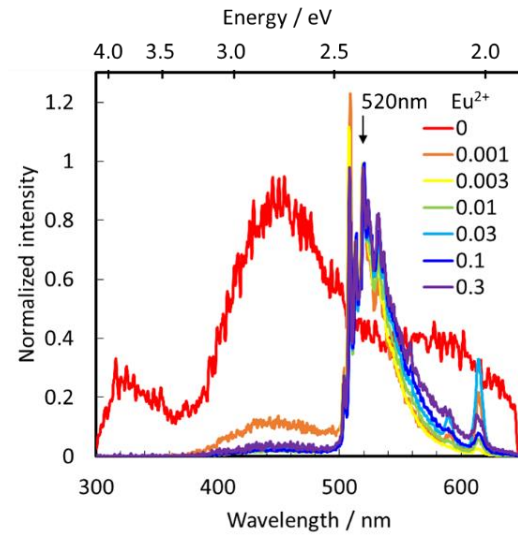


Figure 2.

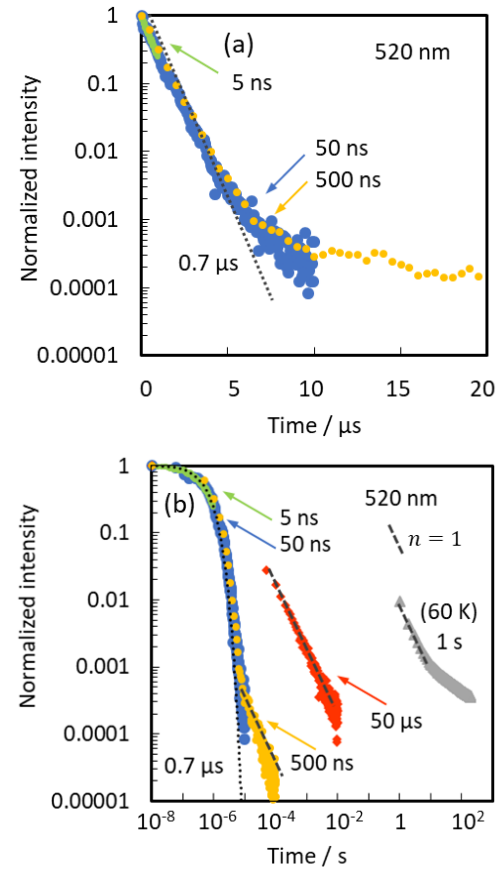


Figure 4.

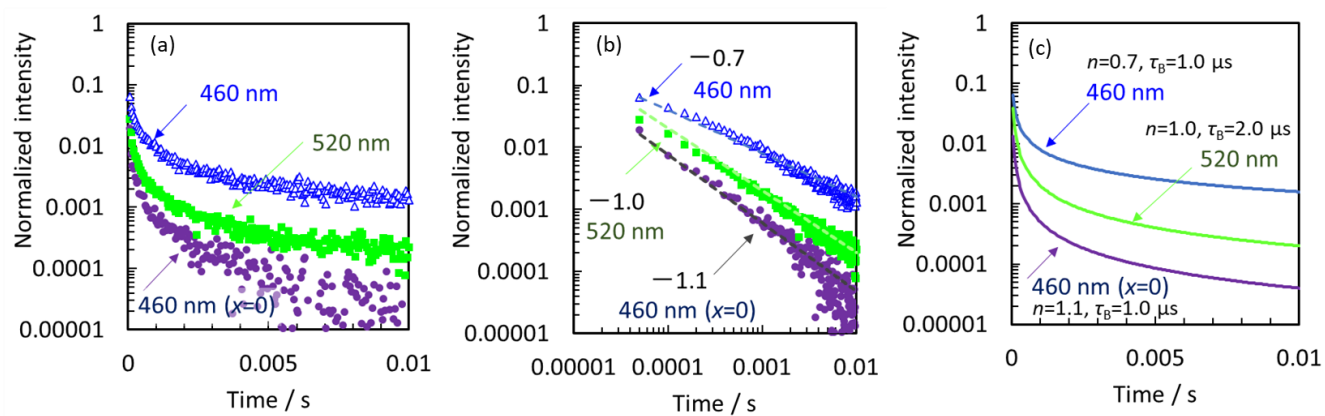


Figure 5.

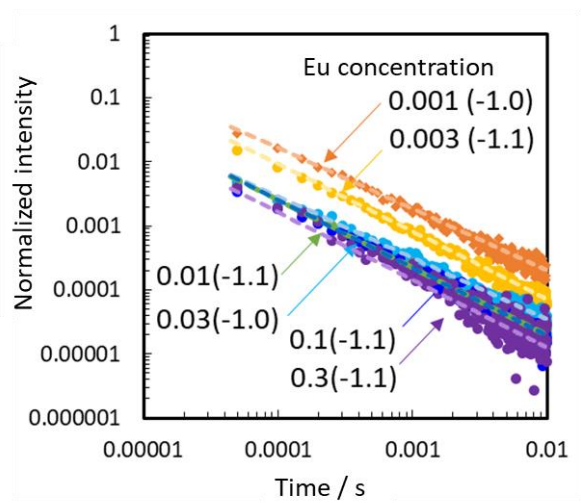


Figure 6.

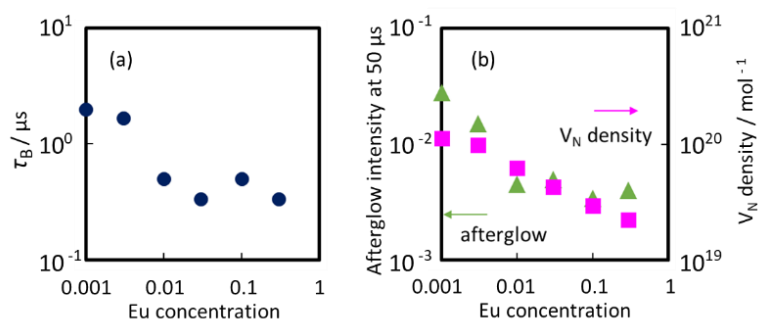


Figure 7.

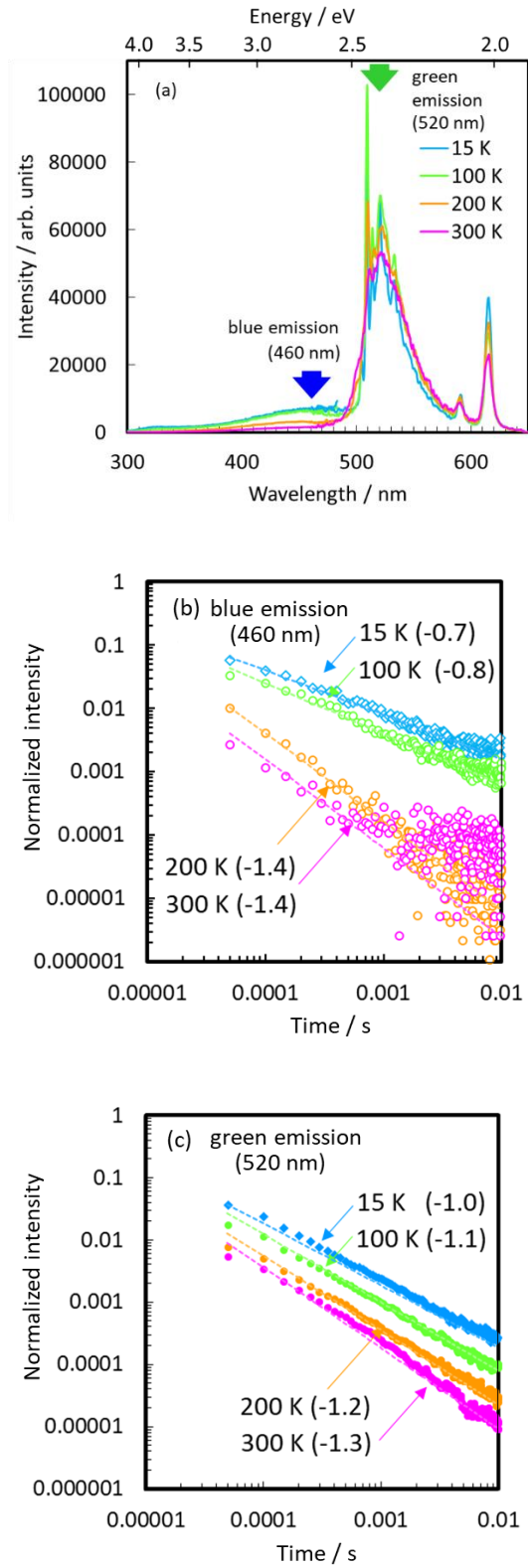


Figure 8.

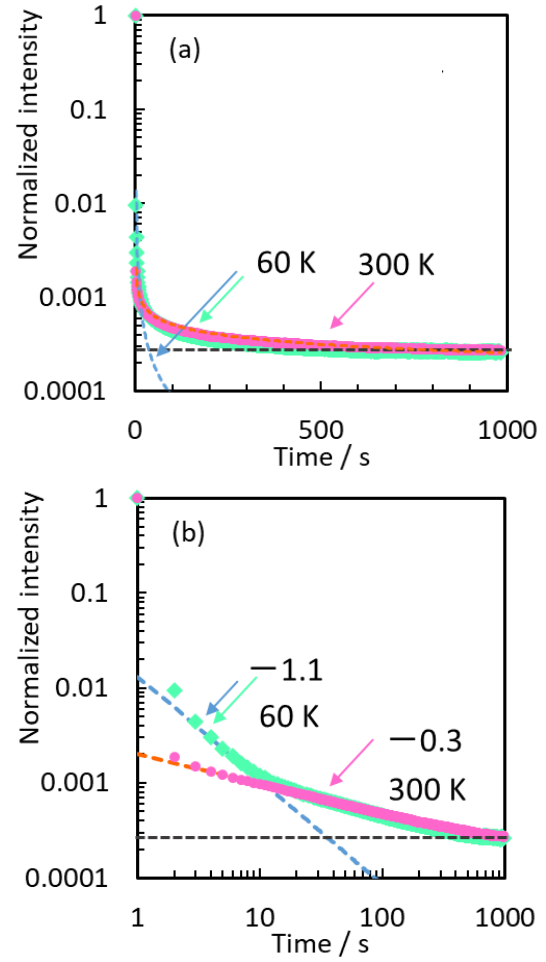


Figure 9.

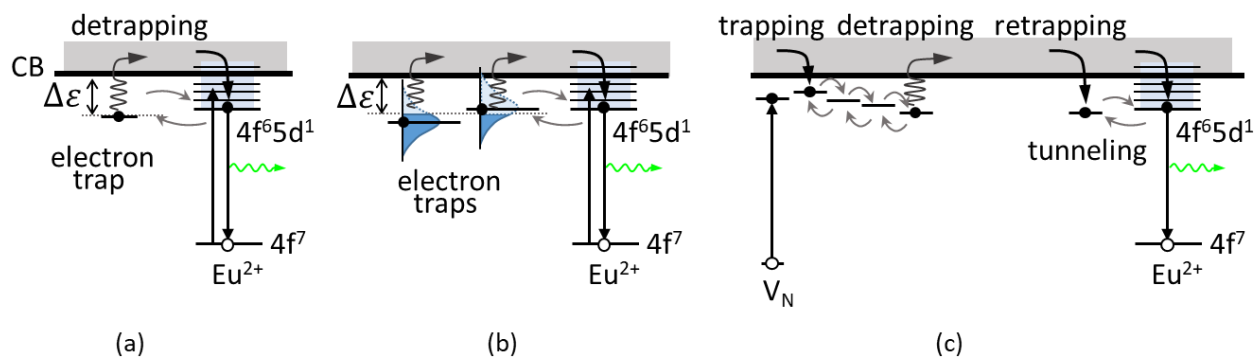


Figure 10.

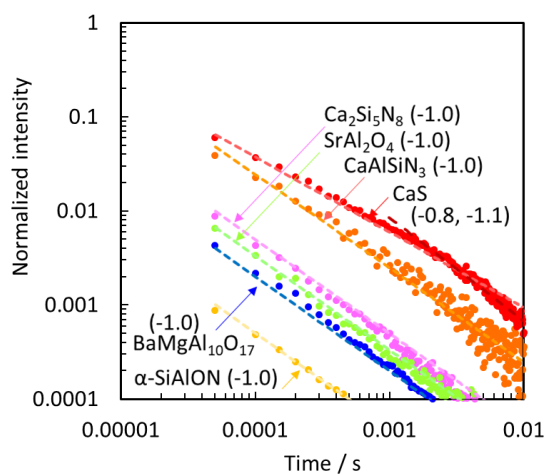


Figure 11.

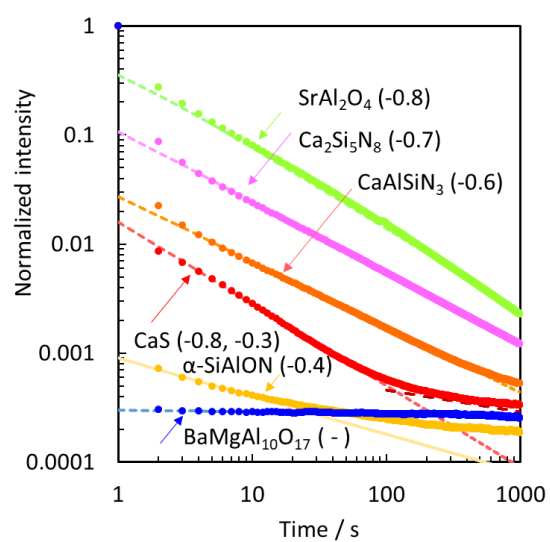


Figure 12.

Tables

Table 1. Decay parameters of β -SiAlON:Eu²⁺ at 15 K. λ is the center wavelength of the measurement. I/I_0 is the ratio of the luminescence intensity at $t = 50 \mu\text{s}$ to the intensity at $t = 0 \text{ s}$. n is the decay power. τ_B is the decay time in Equation (2). τ is the intrinsic decay time in Equation (1) of Eu²⁺ in β -SiAlON:Eu²⁺.

host	x	blue emission				green emission				Eu ²⁺
		λ	I/I_0	n	τ_B	λ	I/I_0	n	τ_B	
		/ nm	50 μs		/ μs	/ nm	50 μs		/ μs	/ μs
β -SiAlON	0	460	0.018	1.1	1.0	510	0.028	1.0	2.0	0.6
	0.001	445	0.008	0.7	1.0	510	0.015	1.1	1.7	0.6
	0.003					520	0.004	1.1	0.5	0.7
	0.01					520	0.005	1.0	0.3	0.8
	0.03					520	0.003	1.1	0.5	0.8
	0.1					520	0.004	1.1	0.3	0.7
	0.3									

Table 2. Temperature dependence of decay parameters of β -SiAlON:Eu²⁺ ($x = 0.001$). Peak intensities at 430–445 nm for blue emission and 510–520 nm for green emission are obtained.

host	x	Temperature / K	blue emission			green emission		
			λ	n	τ_B	λ	n	τ_B
			/ nm		/ μs	/ nm		/ μs
β -SiAlON	0.001	15	445	0.7	1.0	510	1.0	2.0
	0.001	100	440	0.8	1.0	510	1.1	2.0
	0.001	200	440	1.4	2.0	510	1.2	1.4
	0.001	300	430	1.4	1.0	520	1.3	1.4

Table 3. Decay parameters of Eu²⁺-doped phosphors. For TR-F measurement, the excitation wavelength is 266 nm, and the temperature is 15 K. The emission peak wavelength is shown as λ . The intrinsic decay time of Eu²⁺ is shown as τ in Equation (1). I/I_0 is the ratio of the luminescence intensity at $t = 50 \mu\text{s}$ to $t = 0 \text{ s}$. n is the decay power, and τ_B is the decay time in Equation (2). For 1–1000 s, afterglow decay curves are measured at 300 K, and the excitation is conducted by a 254 nm Hg lamp.

host	Eu ²⁺	Tm ³⁺	TR-F measurement						1 - 1000 s	
			λ	τ	I/I_0	n	τ_B	n	τ_B	
	x		/ nm	/ μs	50 μs		/ μs		/ s	
β -SiAlON	0.001	-	510	0.6	0.028	1.0	2.0	0.3	-	
BaMgAl ₁₀ O ₁₇	1.4%	-	450	1.0	0.004	1.0	0.2	-	-	
SrAl ₂ O ₄		Dy ³⁺	520	1.6	0.007	1.0	0.3	0.8	0.3	
α -SiAlON		-	580	0.6	0.001	1.0	0.1	0.4	-	
Ca ₂ Si ₅ N ₈	0.5%	0.5%	615	0.8	0.009	1.0	0.5	0.7	0.03	
CaAlSiN ₃	0.01%	-	635	0.4	0.039	1.0	2.5	0.6	-	
CaS	0.01%	2%	650	0.8	0.060	0.8	1.7	0.8	0.01	